Direct Retrieval of Snow Water Equivalent (SWE) Using the Sentinel-1 Interferometric Phase Response of an Active Reflector

Paolo Perret[1,3], Guido Luzi[2], Pedro Espín-López[2], Martina Lodigiani[3], Lorenzo Silvestri[1], Tommaso Congiu[3], Fabrizio Troilo[3], Francesco Zucca[4], Marco Pasian[1]

[1] University of Pavia, Dept. of Electrical, Computer Science and Biomedical Engineering, Italy
paolo.perret01@universitadipavia.it, (marco.pasian, lorenzo.silvestri)@unipv.it
[2] Centre Tecnològic de Telecomunicacions de Catalunya (CTTC/CERCA), Castelldefels, Spain
gluzi@cttc.es, pedro.espin@cttc.es
[3] Fondazione Montagna Sicura, Courmayeur, Italy
(pperret, mlodigiani, ftroilo, tcongiu)@fondms.org
[4] University of Pavia, Dept. of Earth and Environment Sciences, Italy
francesco.zucca@unipv.it

Keywords: InSAR, Snow Water Equivalent, Active Reflector, Sentinel-1, Alpine snowpack, Interferometry

Abstract

Accurate estimation of Snow Water Equivalent (SWE) from satellite platforms remains one of the most complex challenges in cryospheric remote sensing, primarily limited by temporal coherence loss over natural surfaces and the complex dielectric interaction of radar signals with heterogeneous snowpacks. While C-band Interferometric Synthetic Aperture Radar (InSAR) has demonstrated theoretical potential for detecting snow accumulation via refractive phase delays, its operational application is often hindered by decorrelation phenomena and the instability of natural targets in alpine environments. Active Reflectors (AR), electronic devices traditionally employed for radiometric calibration and geodetic stability monitoring, have not yet been fully exploited for direct snowpack characterization. This study presents a novel methodological approach based on the installation of a C-band Active Reflector positioned flush with the ground surface, allowing natural snow accumulation directly over the device. The system, designed for operation with the Sentinel-1 constellation, integrates separate receiving and transmitting patch antennas with 42 dB radio frequency amplification, ensuring a stable phase response and dominant backscatter signal. The experimental campaign, conducted in Courmayeur (Italy) during the winter of 2024–2025, validated the system capability to provide point-scale SWE measurements through interferometric phase analysis. The system successfully tracked the evolution of the snowpack, measuring a peak SWE of approximately 250 mm, in close agreement with the in situ measurements. Statistical analysis reveals a high correlation between estimated and ground truth values ($R^2 > 0.93$) for both Sentinel-1 descending relative orbits 066 and 139, with a Root Mean Square Error (RMSE) generally below 26 mm. These results indicate that this technology, by overcoming the logistical limitations of passive reflectors, can provide essential calibration nodes for future SAR missions and for data assimilation in hydrological models.

1. Introduction

The seasonal snowpack serves as a critical natural reservoir within the global hydrological cycle, storing precipitation during winter months and releasing it gradually through spring and summer (Barnett et al., 2005). This delayed release sustains water supplies for agriculture, hydropower generation, and domestic consumption across vast regions of the world. Snow Water Equivalent (SWE), defined as the depth of water that would result from the instantaneous melting of the snowpack, represents the fundamental variable for hydrological management, flood forecasting, and water resource assessment (Sturm et al., 2010). However, quantifying SWE with adequate spatial and temporal resolution in complex alpine terrain remains a significant technological challenge.

Traditional in-situ measurement techniques, including snow pillows and manual coring surveys, provide accurate point-scale data but suffer from inherently sparse distribution due to logistical constraints associated with accessing remote mountainous terrain (Smith et al., 2017). Conversely, satellite-based remote sensing approaches offer broad spatial coverage but face substantial limitations. Optical sensors can only retrieve Snow Cover Extent (SCE) and cannot determine snowpack mass (Dozier et al., 2016), while passive microwave radiometry is constrained by coarse spatial resolution (typically exceeding 25 km) and signal saturation in deep snow conditions (Tsang et al., 2000).

Synthetic Aperture Radar (SAR), and specifically Differential Interferometry (DInSAR), offers a promising alternative for SWE estimation. The physical basis of this approach relies on the refraction of radar waves propagating through dry snow, which introduces a phase delay proportional to the SWE content (Guneriussen et al., 2001). This theoretical relationship has been refined to a linear approximation valid for dry snow conditions, enabling direct SWE retrieval from interferometric phase shifts (Leinss et al., 2015). Despite this potential, operational C-band InSAR applications using sensors such as Sentinel-1 are severely limited over natural surfaces due to temporal decorrelation caused by snow metamorphism, wind redistribution, and vegetation interactions (Lievens et al., 2022).

To ensure reliable phase measurements in the presence of decorrelation, Artificial Corner Reflectors (CRs) have been widely employed as stable phase references. However, passive CRs operating at C-band require large physical dimensions, typically exceeding 1.5 m in side length, to achieve sufficient Radar

Cross Section (RCS) and overcome background clutter (Garthwaite, 2017). These dimensions render passive reflectors difficult to deploy and maintain in avalanche-prone terrain. Furthermore, standard corner reflectors must be kept free of snow accumulation to function correctly, which fundamentally prevents measurement of the snow column directly above the target itself.

This study proposes a novel approach to overcome these limitations through the deployment of a compact C-band Active Reflector (AR) installed flush with the ground surface. Unlike passive reflectors that rely solely on geometric properties, ARs employ electronic amplification to provide high RCS with a substantially reduced physical footprint (Luzi et al., 2020). By positioning the device at ground level and allowing snow to accumulate naturally over its surface, we exploit the AR not merely as a geodetic reference point, but as an active probe for the dielectric properties of the overlying snowpack. This paper presents the system design, the theoretical framework for SWE retrieval, and the results from a validation campaign conducted in the Italian Alps during the 2024–2025 winter season.

2. System Design

2.1 Active Reflector Architecture

The instrument employed in this study is a low-cost C-band Active Reflector prototype developed for Sentinel-1 interferometric applications. Unlike passive trihedral corner reflectors, which rely exclusively on geometric properties to redirect incident radar energy back toward the sensor, the AR architecture incorporates a radio frequency (RF) chain to receive, amplify, and retransmit the incoming signal (Luzi et al., 2020). The robustness of this design has been experimentally verified, demonstrating high radiometric reliability and long-term phase stability suitable for precise deformation monitoring (Luzi et al., 2025).

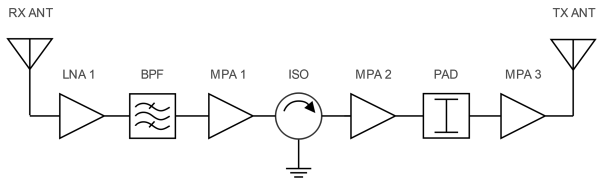

Figure 1. Block diagram of the Active Reflector RF chain illustrating the signal amplification path from RX to TX antennas.

The system, schematically illustrated in Figure 1, operates at the Sentinel-1 center frequency of 5.405 GHz. Internally, the signal received by the antenna passes through a Low-Noise Amplifier (LNA1), a Band-Pass Filter (BPF), and a series of Medium-Power Amplifiers (MPA1–MPA3) including an isolator (ISO) and an attenuator pad (PAD). The device employs two spatially separated microstrip patch array antennas for reception (RX) and transmission (TX), configured to maximize isolation between the two channels. Each antenna consists of a 4×4 element array providing approximately 17 dBi gain. Although the standard architecture typically employs linear (VV) polarization (Pérez et al., 2022), for this study the system was configured to operate in cross-polarization (VH) mode. The electronic RF chain applies a total gain of approximately 42 dB to the received signal before retransmission. The combination of the active gain and the VH configuration ensures a good Signal-to-Clutter Ratio (SCR), exploiting the lower natural backscatter of snow-covered terrain in the cross-polarized channel to keep the point target clearly visible even when attenuated by an overlying snow layer.

The compact form factor represents a key advantage of the active approach. The entire device is housed in a rugged waterproof enclosure measuring approximately $52 \times 32 \times 7$ cm, which is substantially smaller than the equivalent passive reflector that would be required to achieve comparable RCS. For reference, a passive trihedral corner reflector providing equivalent backscatter intensity at C-band would require a side length exceeding 1.7 m (Garthwaite, 2017, Czikhardt et al., 2022). The low power consumption of the system, remaining below 0.6 W during continuous operation, enables autonomous deployment using a 12 V battery buffered by a small solar panel, making the device suitable for extended monitoring campaigns in remote alpine locations (Luzi et al., 2020).

2.2 Installation Configuration

The AR was deployed in a flat open field in Courmayeur, Italy (45.82024°N, 6.96344°E), at an elevation of 1450 m above sea level. This site is characterized by reliable seasonal snow cover and was selected to minimize topographic complexity during the initial validation phase.

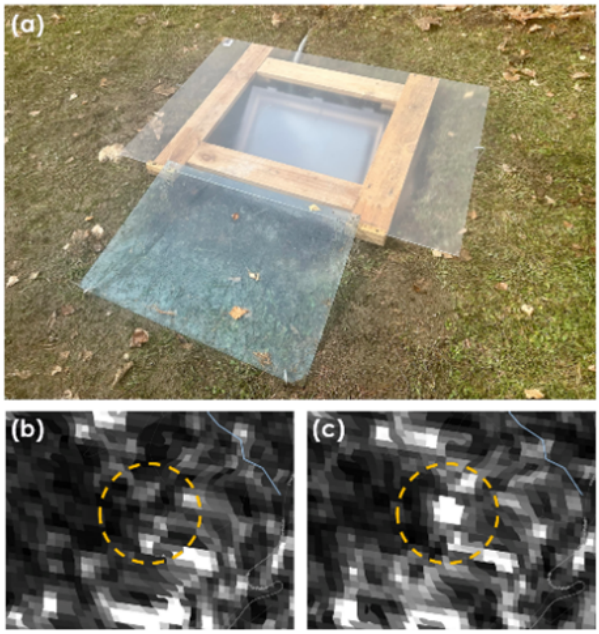

Figure 2. Experimental setup: (a) flush-mounted installation; (b) Sentinel-1 amplitude before installation (about -10 dB) and (c) amplitude after activation (about 2.9 dB) showing the target response.

The deployment configuration was specifically adapted to minimize the interaction between the physical structure and the wind-driven snow redistribution. To achieve this, the AR was installed within an excavated pit, allowing the device to be positioned below the natural ground surface. The pit opening was covered by a rigid polycarbonate sheet aligned flush with the surrounding terrain, as shown in Figure 2(a). This buried setup allows snow to accumulate naturally on the protective interface without the aerodynamic disturbances typical of elevated structures, such as wind scouring and preferential drifting, ensuring

that the snow layer overlying the sensor is representative of the local snowpack.

Inside the protective enclosure, the device was mounted on a tilting bracket to face the Sentinel-1 descending viewing geometries corresponding to relative orbit numbers 066 and 139. The antenna boresight was aligned to the nominal incidence angle of approximately 34° to maximize the received signal strength, while remaining physically protected by the flush-mounted cover. The impact of the device on the SAR image is evident in Figure 2(c), where the target appears as a strong bright pixel (highlighted by the yellow circle) compared to the background clutter visible in the pre-installation image in Figure 2(b). Power was supplied continuously throughout the winter season by the solar-battery system described above, ensuring uninterrupted operation during the entire snow accumulation period.

3. Methodology

3.1 Interferometric SAR Processing

The interferometric analysis utilized Sentinel-1 Interferometric Wide (IW) Single Look Complex (SLC) products acquired on Sentinel-1 descending relative orbits 066 and 139. The processing workflow was implemented using the ESA Sentinel Application Platform (SNAP) software and followed established InSAR procedures adapted for point-target analysis.

The coregistration of image pairs was performed using precise orbit ephemerides provided by the European Space Agency. It is worth noting that during the observation period (winter 2024–2025), the revisit time for the specific relative orbits was limited to 12 days. This was due to the unavailability of Sentinel-1B and the fact that Sentinel-1C, although launched in December 2024, was still in its commissioning phase and not yet fully integrated into the operational interferometric cycle. Interferograms were then generated by computing the complex phase difference $\Delta\phi$ between a reference acquisition and subsequent acquisitions. For each interferometric pair, the chronologically earlier acquisition was designated as the primary image, while the later acquisition was defined as the secondary image. The primary scene used as the absolute reference was selected from a late autumn acquisition to ensure the ground was completely free of snow cover.

Phase values were extracted from the single pixel corresponding to the AR coordinates in each interferogram. Critically, no spatial filtering or multilooking was applied to this pixel to preserve the point-target phase integrity. While multilooking is routinely applied in InSAR processing to reduce phase noise over distributed scatterers, it would degrade the precise phase information available from a high-SCR point target such as the AR.

3.2 SWE Retrieval from Interferometric Phase

The retrieval of SWE relies on isolating the specific phase delay induced by the refraction of radar waves within the snowpack. When a radar signal traverses a dry snow layer, its propagation velocity is reduced relative to free space due to the dielectric properties of the snow medium. This velocity reduction manifests as an additional phase accumulation proportional to the snow mass encountered along the propagation path.

Following the standard functional model for radar interferometry (Hanssen, 2001), the total interferometric phase $\Delta\phi_{int}$ measured by the sensor can be expressed as a summation of several contributions:

$$\Delta\phi_{int} = \Delta\phi_{geom} + \Delta\phi_{atm} + \Delta\phi_{snow} + \Delta\phi_{noise} \quad (1)$$

where $\Delta\phi_{geom}$ accounts for orbital and topographic fringes, $\Delta\phi_{atm}$ represents the atmospheric path delay difference, $\Delta\phi_{snow}$ is the refraction phase shift due to the snow layer, and $\Delta\phi_{noise}$ includes thermal noise and decorrelation terms. In our processing chain, implemented using the ESA Sentinel Application Platform (SNAP) Graph Processing Tool, the geometric components were removed through precise orbit application and DEM-based topographic phase subtraction. The atmospheric contribution was compensated by computing the differential phase between the Active Reflector and a nearby Persistent Scatterer (PS) located on a snow-free structure (45.80655°N, 6.96486°E, 1244 m a.s.l.), at a distance of about 1.5 km from the AR site. At this separation, atmospheric phase screens are expected to be largely common-mode at the repeat-pass scale and are therefore strongly reduced by differencing. Residual spatial variability in atmospheric delay is therefore absorbed into the $\Delta\phi_{noise}$ term and contributes to the retrieval uncertainty, while only the AR is expected to exhibit a snow-induced phase term.

Following the physical model described in the literature (Bovenga et al., 2025, Leinss et al., 2015), the relationship between the isolated snow phase and the Snow Water Equivalent is given by:

$$\Delta\mathrm{SWE} = \frac{\Delta\phi_{snow} \cdot \lambda}{2\pi \cdot \beta \cdot (1.59 + \theta^{2.5})} \quad (2)$$

where λ is the radar wavelength (approximately 5.6 cm for Sentinel-1 C-band), θ is the local incidence angle relative to the ground normal expressed in radians, extracted at the AR pixel, and β is a dimensionless optimization parameter. Following the sensitivity analysis presented in literature (Bovenga et al., 2025), we assume $\beta = 1$. The constant 1.59 is empirically determined (Leinss et al., 2015) and derives from the computation of the dielectric permittivity of dry snow for low density conditions. Equation 2 yields ΔSWE in meters, provided that λ is expressed in meters. For consistency, all ΔSWE values are converted and reported in millimeters in the remainder of the paper.

A critical challenge inherent to C-band interferometry is phase ambiguity, as the high sensitivity of the signal results in rapid phase wrapping. As discussed in previous studies (Guneriussen et al., 2001), the interferometric phase is wrapped within the interval $[-\pi, +\pi]$, meaning that a full 2π cycle corresponds to a relatively small change in SWE (approximately 30 mm in our configuration). To address this, we adopted a supervised phase unwrapping strategy constrained by auxiliary data. The phase evolution was cross-referenced with the periodic in-situ SWE measurements to manually determine the correct number of 2π cycles to be added to the wrapped phase. While a supervised process was employed for this prototype, automated unwrapping strategies could be implemented in future operational workflows.

3.3 Wet Snow Detection and Quality Control

While the interferometric phase provides quantitative SWE estimates under dry snow conditions, the presence of liquid water in the snowpack fundamentally alters the radar interaction and invalidates the refraction-based retrieval model. The radiometric information contained in the backscatter intensity offers a complementary diagnostic capability: the detection of wet snow conditions that would compromise phase-based measurements.

The physical basis for wet snow detection relies on the strong absorption of C-band microwave radiation by liquid water. When the volumetric liquid water content exceeds approximately 1%, the real part of the dielectric permittivity of the snow medium increases, while the imaginary part becomes positive, causing substantial signal attenuation (Nagler and Rott, 2000). This characteristic drop in backscattering intensity is a well-documented proxy for identifying the onset of the moistening phase in alpine snowpacks (Marin et al., 2020). Furthermore, the specific sensitivity of the Sentinel-1 cross-polarized channel (VH) to liquid water content has been documented as an effective indicator for detecting the onset of the melting phase (Nagler et al., 2016). This absorption reduces the penetration depth from several meters in dry snow to less than one meter in wet conditions, effectively preventing the radar signal from reaching the underlying ground surface.

To filter out unreliable acquisitions, we monitored the radiometrically calibrated backscatter intensity extracted at the AR pixel (reported as σ^0 in dB for convenience) throughout the season. Since the AR behaves as a dominant point target, this single-pixel calibrated intensity provides a robust proxy for signal strength and a practical quality-control indicator. A rigorous absolute RCS estimation could be obtained by integrating the calibrated intensity over a window encompassing the full impulse response (main lobe and side lobes). However, for wet-snow gating we only require a stable and repeatable intensity metric, which is satisfied by the AR-pixel time series. We established an intensity threshold of $\sigma^0 = -7.5$ dB (VH polarization) to discriminate between dry snow (high transmissivity) and wet snow (high absorption) conditions. This value was empirically selected considering the background backscattering levels recorded at the site prior to the AR installation, ensuring that the analysis relies only on acquisitions where the AR signal remains dominant over the background clutter. Additionally, a coherence threshold of $\gamma = 0.3$ was applied to discard phase measurements corrupted by severe temporal decorrelation. This limit was determined based on an *a posteriori* analysis of the dataset, corresponding to the average coherence level observed during the wet snow phase where the liquid water content compromised phase stability. Consequently, acquisitions falling below these established radiometric and interferometric thresholds were classified as unreliable, serving as indicators of wet snow presence and the potential onset of the melting season.

4. Results

4.1 Radiometric Stability and Melting Detection

The analysis of the backscatter intensity (σ^0) provides critical insights into the physical state of the snowpack and the operational status of the Active Reflector. Figure 3 illustrates the temporal evolution of σ^0 for both monitored orbits (066 and 139) spanning from November 2024 to April 2025.

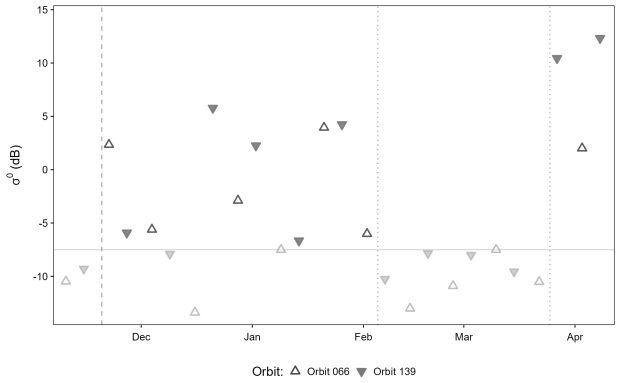

Figure 3. Temporal evolution of the Backscattering Coefficient (σ^0) for Orbits 066 and 139 (VH polarization) encompassing the accumulation and melting phases.

Following the installation on November 20, 2024 (marked by the dashed vertical line), the backscatter response remained stable and high, generally fluctuating between -5 and +5 dB during the accumulation phase (December and January). This stability confirms that dry snow is largely transparent to C-band radiation, allowing the AR to maintain a strong return signal despite being buried under more than a meter of snow.

A sharp transition is observable starting in early February 2025. This period was identified as the onset of the melting phase (delimited by the dotted vertical lines), characterized by diurnal freeze-thaw cycles that result in significant signal attenuation. From this time onwards, we observe a drastic reduction in σ^0, with values frequently dropping below the -7.5 dB threshold (indicated by the grey horizontal line). This attenuation is characteristic of wet snow, where the presence of liquid water increases the dielectric loss, leading to strong signal absorption. Intensity drops reaching values as low as -13 dB are scattered throughout the observation period from February onwards, suggesting recurrent episodes of high liquid water content within the snowpack. Finally, the cessation of the melting phase is observed in early April (second dotted vertical line). With the complete depletion of the snow cover, the attenuation vanishes, and the backscatter intensity exhibits a sharp recovery to high positive values (exceeding 10 dB for Orbit 139), confirming the return to free-space propagation conditions.

4.2 Interferometric Coherence Analysis

Parallel to the intensity analysis, the interferometric coherence serves as a proxy for the phase quality. Figure 4 displays the coherence time series extracted at the AR coordinates for the cross-polarized channel (VH).

During the dry snow period (November–January), coherence values for Orbit 066 generally remained above the reliability threshold of 0.3 (indicated by the horizontal line), oscillating between 0.4 and 0.7. This demonstrates that the AR preserves sufficient phase stability even under snow cover, despite the volume scattering effects introduced by the snowpack. Orbit 139 exhibits a compatible trend, confirming the usability of the signal for interferometric processing.

Conversely, the melting phase exhibits a general decrease in coherence stability. While values do not systematically col-

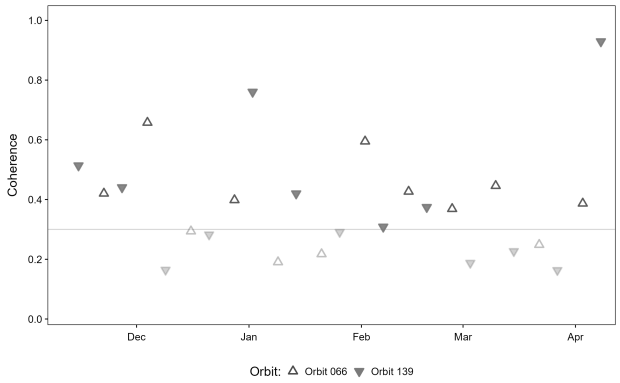

Figure 4. Interferometric coherence time series extracted at the AR coordinates (VH polarization), with the reliability threshold marked at 0.3.

lapse, they more frequently approach or fall below the acceptance threshold compared to the dry snow period.

It is worth noting that some low-coherence events in December and January correspond to heavy snowfall episodes occurring between satellite passes, which alter the scattering center geometry and introduce volume decorrelation. However, unlike natural terrain, the high Signal-to-Clutter Ratio of the AR allows for coherence recovery once the snowpack stabilizes. Finally, towards the end of the campaign in April, the complete depletion of the snow cover leads to a restoration of high coherence values (reaching nearly 0.9 for Orbit 139). This recovery confirms the return to snow-free conditions, where the AR acts as a highly stable point scatterer unaffected by the dielectric complexity of the snowpack.

4.3 Phase Evolution and SWE Retrieval

The core result of this study is the retrieval of SWE from the interferometric phase shifts. A crucial step in this process involves resolving the phase ambiguity by determining the correct number of full phase cycles (2π wraps) to add to the measured fractional phase. Figure 5 illustrates the temporal evolution of these integer phase ambiguities (or cycle counts) determined through the supervised unwrapping process.

A clear positive step-wise trend is visible in the integer count from December to early February, corresponding to the progressive accumulation of snow. The count increases reaching up to 3 cycles of delay (where 1 cycle is about 30 mm of SWE) before the onset of melting. This confirms the theoretical expectation that increasing snow mass induces a proportional phase delay exceeding the ambiguity interval. After early February, negative integer cycles were introduced in the supervised processing to track the decreasing SWE trend typical of the melting season. However, the resulting sequence exhibits erratic behavior and sharp discontinuities, confirming that the presence of liquid water invalidates the linear phase-SWE relationship, rendering the retrieval unreliable in this regime.

By applying Equation 2 to the reliable phase data, we derived the SWE time series presented in Figure 6. The InSAR-derived estimates, represented by the dashed lines, are compared against ground truth measurements (black circles). These reference values were obtained through periodic manual snow pit surveys performed in close proximity to the sensor, where snow density and depth were measured to compute the total SWE. The agreement during the accumulation phase is remarkable. Both Orbit 066 and 139 track the ground truth evolution with high fidelity. The system correctly identified the rapid accumulation events in early January and the steady increase throughout the month. The peak accumulation was detected in early February, with the InSAR data estimating approximately 240–250 mm of SWE, slightly underestimating the ground truth peak of about 273 mm.

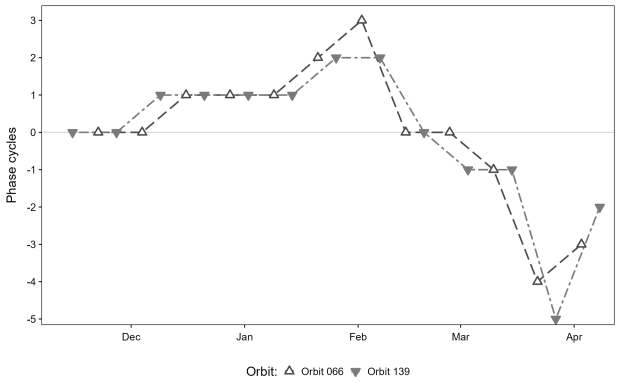

Figure 5. Temporal evolution of the integer phase cycles (number of 2π wraps) added to the wrapped signal to reconstruct the total SWE.

The portion of the time series following early February is visualized with reduced opacity (high transparency) to explicitly mark the transition into the melting phase and wet snow conditions. In this regime, the fundamental assumption of a dry, non-absorptive scattering medium is violated by the presence of liquid water. This causes a divergence between the InSAR-derived estimates and the physical ground truth trend, which underscores the intrinsic limitation of C-band phase retrieval during the melting season and justifies the classification of these data points as not reliable.

4.4 Statistical Validation

To quantify the accuracy of the proposed method, a scatter plot analysis was performed comparing the Sentinel-1 derived SWE against the interpolated Ground Truth data for the valid observation window (Figure 7). In this visualization, the error bars represent the uncertainty associated with the ground measurements.

The statistical metrics indicate a strong agreement between the InSAR-derived estimates and the interpolated ground truth. Orbit 139 exhibited a high correlation, characterized by a coefficient of determination $R^2 = 0.962$ and a Root Mean Square Error (RMSE) of 19.2 mm. Comparable results were obtained for Orbit 066, with an $R^2 = 0.936$ and an RMSE of 25.6 mm. Both orbits exhibit a slight negative bias (approximately -12.5 mm for Orbit 139 and -16.9 mm for Orbit 066), indicating a systematic underestimation of the total snow mass. This underestimation could be attributed to the linear approximation of the refractive index used in Equation 2, which might not fully account for the densification of the snowpack at the bottom layers. Nevertheless, the bias remains well within the typical error margins of manual field measurements, suggesting that the active reflector approach is viable for operational monitoring.

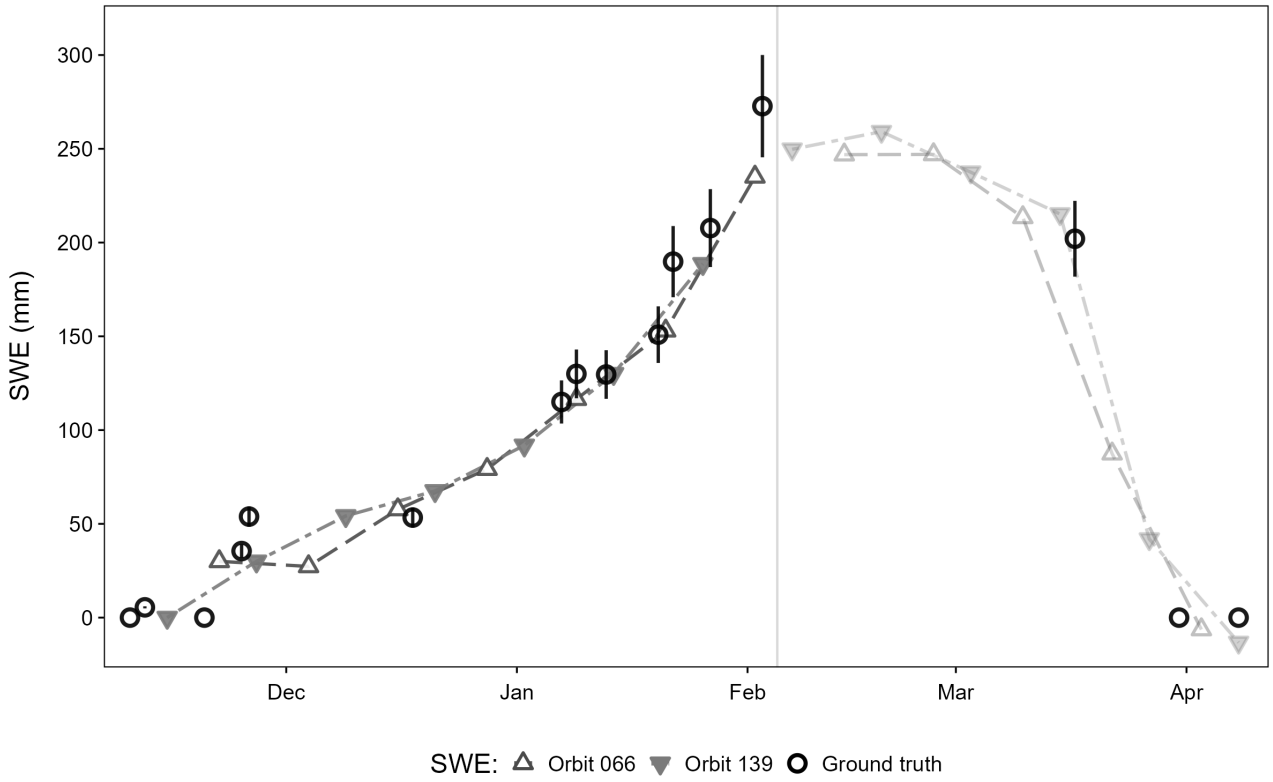

Figure 6. Comparison of SWE time series derived from InSAR (dashed lines) versus Ground Truth (black circles). The vertical grey line marks the onset of the melting phase.

5. Discussion

The results presented in this study demonstrate the viability of using ground-flush Active Reflectors for direct SWE monitoring from spaceborne SAR platforms. This approach offers several advantages over both conventional in-situ methods and passive reflector installations.

From a logistical perspective, the compact dimensions and low weight of the AR substantially simplify deployment compared to large passive corner reflectors. The results from Figure 3 highlight a crucial operational advantage: the active amplification (approx. 42 dB) allows the target to remain visible even under significant snow loads, a capability that passive reflectors of comparable size cannot match.

From a measurement perspective, the flush configuration enables direct sensing of the snow column overlying the target. The high correlation ($R^2 > 0.93$) observed in Figure 7 validates the phase-delay model for dry snow. The discrepancy between InSAR and ground truth appearing after the beginning of February (Figure 6) serves as a distinct indicator of the phase transition in the snowpack. While this limits the capability to measure peak SWE during the wet spring season, the combination of phase and amplitude analysis turns the AR into a dual-sensor: a quantitative SWE gauge during winter and a precise wet-snow detector during spring. The primary limitation of the current implementation remains the phase ambiguity inherent to C-band. While this study adopted a supervised unwrapping approach, future operational workflows will benefit significantly from the restoration of the Sentinel-1 constellation's full capacity. With the operational activation of Sentinel-1C, the revisit time is reduced from 12 to 6 days. This higher temporal sampling is expected to mitigate temporal decorrelation and reduce phase unwrapping errors, as the smaller phase accumulation between shorter intervals decreases the likelihood of exceeding ambiguity limits. Additionally, automated workflows could integrate real-time snow depth data from local automatic weather stations (AWS) to constrain the phase unwrapping process. Furthermore, the signal degradation during wet snow conditions represents a physical constraint. Future work will focus on extending this technology to L-band missions currently under development, including NISAR and ROSE-L, where the longer wavelength of approximately 24 cm will significantly increase the unambiguous SWE range per wrap (Tsang et al., 2022), and potentially offer better penetration in moist snow conditions.

6. Conclusions

This study has demonstrated that low-cost, flush-mounted Active Reflectors can provide reliable, direct measurements of Snow Water Equivalent using Sentinel-1 C-band InSAR. The active amplification architecture ensures target visibility through the attenuating snowpack, overcoming the logistical and physical limitations of large passive corner reflectors. The experimental campaign in Courmayeur, Italy, validated the system's capability to track snowpack evolution throughout the 2024–2025 winter season. The statistical analysis of the field data confirms the precision of the method, yielding an RMSE of approximately 19–25 mm compared to manual ground truth. We successfully identified the transition from dry to wet snow using radiometric thresholds ($\sigma^0 < -7.5$ dB), which is critical for masking unreliable phase data. While C-band phase ambiguity requires careful management through constrained temporal unwrapping, the proposed configuration offers a prac-

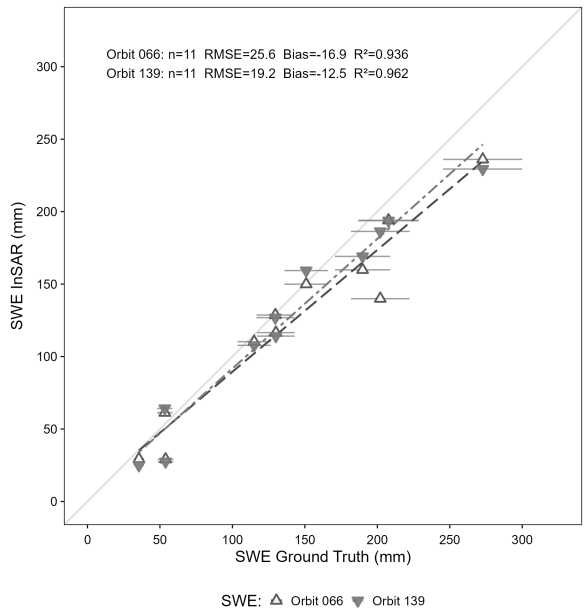

Figure 7. Scatter plot of InSAR-derived SWE versus Ground Truth. Linear regression statistics are reported for Orbits 066 and 139.

tical and scalable approach for establishing calibration nodes in alpine environments. Integration with upcoming L-band SAR missions will further enhance measurement capability by reducing phase wrapping issues and potentially enabling unassisted phase retrieval over a wider range of snow conditions.

Acknowledgements

This research was supported by Fondazione Montagna Sicura. The authors acknowledge the European Space Agency and the Copernicus programme for providing Sentinel-1 SAR data.

References

Barnett, T. P., Adam, J. C., Lettenmaier, D. P., 2005. Potential impacts of a warming climate on water availability in snow-dominated regions. *Nature*, 438, 303–309.

Bovenga, F., Belmonte, A., Refice, A., Argentiero, I., 2025. Multi-Band Differential SAR Interferometry for Snow Water Equivalent Retrieval over Alpine Mountains. *Remote Sensing*, 17(14), 2479. https://doi.org/10.3390/rs17142479.

Czikhardt, R., van der Marel, H., van Leijen, F. J., Hanssen, R. F., 2022. Estimating Signal-to-Clutter Ratio of InSAR Corner Reflectors From SAR Time Series. *IEEE Geoscience and Remote Sensing Letters*, 19, 1–5.

Dozier, J., Bair, E. H., Davis, R. E., 2016. Estimating the spatial distribution of snow water equivalent in the world's mountains. *WIREs Water*, 3(3), 461–474.

Garthwaite, M. C., 2017. On the Design of Radar Corner Reflectors for Deformation Monitoring in Multi-Frequency InSAR. *Remote Sensing*, 9(7), 648.

Guneriussen, T., Høgda, K. A., Johnsen, H., Lauknes, I., 2001. InSAR for estimation of changes in snow water equivalent of dry snow. *IEEE Transactions on Geoscience and Remote Sensing*, 39(10), 2101–2108.

Hanssen, R. F., 2001. *Radar Interferometry: Data Interpretation and Error Analysis*. Remote Sensing and Digital Image Processing, 2, Springer, Dordrecht, The Netherlands.

Leinss, S., Wiesmann, A., Lemmetyinen, J., Hajnsek, I., 2015. Snow Water Equivalent of Dry Snow Measured by Differential Interferometry. *IEEE Journal of Selected Topics in Applied Earth Observations and Remote Sensing*, 8(8), 3773–3790.

Lievens, H., Brangers, I., Marshall, H.-P., Jonas, T., Olefs, M., De Lannoy, G., 2022. Sentinel-1 snow depth retrieval at sub-kilometer resolution over the European Alps. *The Cryosphere*, 16, 159–177.

Luzi, G., Fernandez, E., Mira Pérez, F., Crosetto, M., 2020. A low cost active corner reflector to assist snow monitoring through Sentinel/1 images. *2020 14th European Conference on Antennas and Propagation (EuCAP)*, Copenhagen, Denmark, 1–4.

Luzi, G., Gao, Q., Espín-López, P., 2025. Experimental Study of the Stability of a Low-Cost C-Band Active Reflector Using Sentinel-1 Imagery. *IEEE Access*, 13, 55202–55210.

Marin, C., Bertoldi, G., Premier, V., Callegari, M., Brida, C., Hürkamp, K., Tschiersch, J., Zebisch, M., Notarnicola, C., 2020. Use of Sentinel-1 radar observations to evaluate snowmelt dynamics in alpine regions. *The Cryosphere*, 14(3), 935–956.

Nagler, T., Rott, H., 2000. Retrieval of wet snow by means of multitemporal SAR data. *IEEE Transactions on Geoscience and Remote Sensing*, 38(2), 754–765.

Nagler, T., Rott, H., Ripper, E., Bippus, G., Hetzenecker, M., 2016. Advancements for Snowmelt Monitoring by Means of Sentinel-1 SAR. *Remote Sensing*, 8(4), 348.

Pérez, F. M., Luzi, G., Espín-López, P., 2022. Design and test of a circularly polarized microstrip antenna array for a Sentinel-1 SAR active reflector with co- and cross-polarization capability. *2022 16th European Conference on Antennas and Propagation (EuCAP)*, 1–4.

Smith, C. D., Kontu, A., Laffin, R., Pomeroy, J. W., 2017. An assessment of two automated snow water equivalent instruments during the WMO Solid Precipitation Intercomparison Experiment. *The Cryosphere*, 11, 101–116.

Sturm, M., Taras, B., Liston, G. E., Derksen, C., Jonas, T., Lea, J., 2010. Estimating Snow Water Equivalent Using Snow Depth Data and Climate Classes. *Journal of Hydrometeorology*, 11(6), 1380–1394.

Tsang, L., Chen, C.-T., Chang, A. T. C., Guo, J., Ding, K.-H., 2000. Dense media radiative transfer theory based on quasicrystalline approximation with applications to passive microwave remote sensing of snow. *Radio Science*, 35(3), 731–749.

Tsang, L., Durand, M., Derksen, C., Barros, A. P., Kang, D.-H., Lievens, H., Marshall, H.-P., Zhu, J., Johnson, J., King, J., Lemmetyinen, J., Sandells, M., Rutter, N., Siqueira, P., Nolin, A., Osmanoglu, B., Vuyovich, C., Kim, E., Taylor, D., Merkouriadi, I., Brucker, L., Navari, M., Dumont, M., Kelly, R., Kim, R. S., Liao, T.-H., Borah, F., Xu, X., 2022. Review article: Global monitoring of snow water equivalent using high-frequency radar remote sensing. *The Cryosphere*, 16, 3531–3573.